analytical chemistry

pubs.acs.org/ac Article

Metal–Organic Framework-Functionalized Paper-Based Electrochemical Biosensor for Ultrasensitive Exosome Assay

Xiaojuan Liu, Xin Gao, Limin Yang, Yuecan Zhao, and Feng Li*

Cite This: *Anal. Chem.* 2021, 93, 11792–11799 Read Online

ACCESS | Metrics & More | Article Recommendations | Supporting Information

ABSTRACT: The exosome has emerged as a promising noninvasive biomarker for the early diagnosis of cancer. Therefore, it is highly desirable to develop simple, inexpensive, and user-friendly biosensors for convenient, sensitive, and quantitative exosome assay. Herein, we developed a simple and cost-efficient electrochemical biosensor by combining a metal–organic framework (MOF)-functionalized paper and a screen-printed electrode (SPE) for portable, ultrasensitive, and quantitative determination of cancer-derived exosomes. In principle, the biosensor relied on recognition of the exosome by Zr-MOFs and aptamer to initiate the hybridization chain reaction (HCR) and the formation of DNAzyme for signal amplification. Benefiting from the high signal amplification ability of HCR, the label-free paper-based biosensor is capable of ultrasensitive exosome assay with a detection limit down to 5×10^3 particles/mL, which is superior to that of most reported methods. Moreover, the proposed paper-based biosensor possessed the advantages of low cost, simple operation, and high sensitivity, making it affordable and deliverable for point-of-care (POC) diagnosis in resource-limited settings.

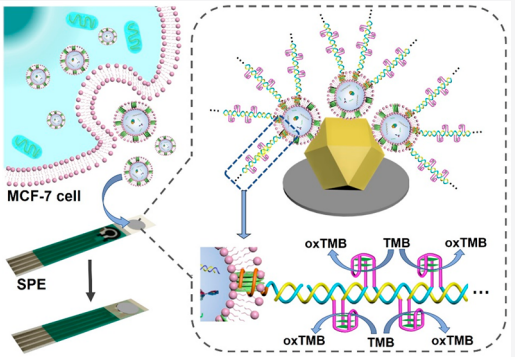

INTRODUCTION

Exosomes are nanoscale membrane-enclosed extracellular vesicles (30–150 nm) shed by various cells, such as leukocytes, dendritic cells, epithelial cells, stem cells, and cancerous cells.[1] Through carrying considerable amounts of DNA, RNA, proteins, and other biomolecules inherited from their parental cells, they are involved in intercellular communication and transfer vital messages into recipient cells to affect the pathological and physiological process.[2−4] As messengers, they are highly stable in circulation and present in many body fluids, such as blood, saliva, urine, cerebrospinal fluid, and so on.[5] Recent reports have proved that tumor cells secrete a larger number of exosomes than normal cells.[6] These cancer-derived exosomes play an important role in tumor metastasis, proliferation, and immune modulation.[7−9] Therefore, exosomes have emerged as a new type of potential biomarker for the noninvasive early cancer diagnosis. When considering the use of exosome as biomarkers, a challenge is their relatively low concentrations in the early stage of disease and the high levels of interfering biomolecules in bodily fluids. Thus, specific recognition and signal amplification are in high demand for the sensitive exosome assay.

To recognize exosomes, some specific proteins (e.g., CD63, EGFR, HER2, EpCAM), which are highly expressed on the phospholipid bilayer of exosome, can be used as promising biomarkers for the detection of cancer-related exosomes.[10,11] Antigen–antibody interaction is one of the most classic recognition methods for identifying these exosomal surface proteins. Based on the immunoreaction, numerous biosensors have been developed by using exosomal proteins as efficacious antigens.[12−14] Compared with antibodies, aptamers, selected via an in vitro systematic evolution of ligands by the exponential enrichment (SELEX) technique, have been utilized as alternatives for the recognition of exosomal surface proteins due to their merits of chemical stability and cost-effectiveness.[15,16] Generally, aptamers are short single-stranded DNA (ssDNA) with high flexibility. Through bending themselves into specific secondary structures, aptamers can bind to their target proteins in a "lock and key" model with excellent specificity and affinity, making them a versatile recognition element for constructing exosome biosensors.[17] Furthermore, binding between the aptamer and its target is an efficient way to trigger the conformational change of the DNA probe, which can be easily integrated with other nucleic acid-based signal transformation and amplification strategies.[18] For example, the recognition between aptamers and exosomal proteins have been designed to trigger the formation of DNA walkers with exosome or nanoparticles as cores for signal amplification.[19−21] Other signal amplification strategies, such as copper-medicated signal amplification,[22] conjugation of

Received: May 31, 2021
Accepted: August 11, 2021
Published: August 19, 2021

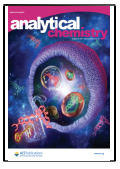

https://doi.org/10.1021/acs.analchem.1c02286
Anal. Chem. 2021, 93, 11792–11799

horseradish peroxidase (HRP)-mediated catalytical amplification,[23,24] steric hindrance-controlled signal amplification,[25] and droplet digital polymerase chain reaction (PCR),[26] have also been combined into an aptasensor for sensitive determination of exosomes. However, most of the reported amplification strategies rely on either the labeling of the oligonucleotides or the bioenzymes, which are expensive or require strict reaction conditions, limiting their extensive applications. Therefore, the development of novel label-free and bioenzyme-free target recognition and signal amplification strategies is highly desirable for the construction of exosome biosensors.

Reading the amplified signals is believed to be another important factor that determines the potential utility of exosome biosensors. Recently, various technologies have been employed in different biosensors for quantifying exosome. For example, surface plasmon resonance,[27−29] surface enhanced Raman scatting (SERS),[30] and mass spectrometry[31] have been used for sensitive determination of exosomes. However, these methods are dependent on expensive equipment and sophisticated operations, thus limiting their wider applications for resource-limited environments. As suggested by the World Health Organization (WHO), developing convenient and reliable point-of-care (POC) diagnostic tools to test the disease-associated biomarkers is of significant importance for improving patient care in developing countries and home healthcare settings. In this regard, colorimetry and fluorescence approaches are the most widely used signal readout strategies in POC diagnostic tools.[32−34] Although these optical methods have been successfully developed for the detection of exosome,[22−25] it is challenging to achieve a quantitative and sensitive assay without the aid of other advanced instruments. Electrochemistry is another powerful technique used in various POC sensors owing to their intrinsic advantages of low cost, portability, high sensitivity, simple operation, rapid response, excellent resistance to color, and ease of miniaturization.[35,36] In our previous work, we have reported paper-based electrochemical POC biosensing tools by integrating DNA-based target recognition and signal amplification strategies onto paper substrates along with commercial screen-printed electrode (SPE)[37] and personal glucose test strips as signal readout elements.[38] Additionally, the electrochemical approach has also been designed for application in exosome research, but the need of immobilizing probes on the electrode surface restricts their potential applications.[39,40] To solve the problem of electrode modification, our group developed homogeneous electrochemical approaches for sensitive determination of exosome.[41,42] However, these homogeneous strategies were carried out in solution, which were not suitable for user-friendly POC tests. Hence, further efforts are still required for designing facile POC diagnostic tools that enable end-users to effectively quantify exosomes in remote areas.

Metal−organic frameworks (MOFs) are a type of synthesized organic/inorganic crystalline nanomaterials self-assembled from organic linkers and metal ions. Their unique features of large surface areas, high porosity, tunable framework structures, and multiple functionalities make them extremely attractive for biosensing applications.[43] For example, the high porosity provides an extra advantage to using MOFs as nanocarriers for encapsulating signal molecules and release them to generate strong signals through target-triggered reaction.[44−46] Furthermore, their high surface areas facilitate their application for adsorbing of abundant functional materials, such as DNA probe, bioenzyme, nanoparticles, and so on.[47,48] In particular, Zr-MOFs can bind strongly to phosphate groups via the formation of Zr−O−P bonds. The high affinity between them has been proved to be an efficient way for selective immobilizing DNA molecules.[49,50]

Inspired by the fact that the outer surface of the exosome's phospholipid bilayer is rich with hydrophilic phosphate head,[51−53] herein, a novel label-free and enzyme-free paper-based POC biosensing tool has been developed for the quantitative exosome assay by using Zr-MOFs and aptamer as the recognition system along with hybridization chain reaction (HCR) for signal amplification. In this biosensor, Zr-MOFs were modified on the surface of paper for capturing exosome via the coordination interaction. Subsequently, CD63, a protein that usually overexpressed on many cancer exosomes' surfaces, was recognized by its aptamer to trigger the conformation change of the DNA probe, initiating the upstream HCR amplification. The double-strands DNA (dsDNA) nanowires produced by HCR reaction were designed to contain numerous hemin/G-quadruples DNAzymes, which can catalyze the oxidation of 3,3′,5,5′-tetramethylbenzidine (TMB), reducing the signal response of TMB on the commercial SPE. By taking advantage of the excellent signal amplification of HCR and the selective recognition ability of Zr-MOFs and aptamer, the developed paper-based exosome biosensor is capable of sensitive and selective determination of tumor-derived exosome. Furthermore, the proposed paper-based electrochemical biosensor is very cheap, and it costs less than $2 per test, making it affordable for the potential applications in resource-limited settings.

EXPERIMENTAL SECTION

Chemicals and Materials. TMB and hemin were purchased from Sigma-Aldrich Trading Co., Ltd. (USA). Zirconium oxide chloride octahydrate ($ZrOCl_2·8H_2O$), 1,4-benzenedicarboxylic acid, and *N*,*N*-dimethylformamide (DMF) were supplied by Shanghai Macklin Biochemical Co., Ltd. (Shanghai, China). All of the chemicals were of analytical reagent grade. The human breast cancer cell line (MCF-7) was bought from Procell Life Science Co., Ltd. (Wuhan, China). Exospin kit was purchased from Shanghai XP Biomed Ltd. (Shanghai, China).

Synthesis of UiO-66 Nanoparticles. The UiO-66 nanoparticles were fabricated through the following procedures: First, benzoic acid (600 mg) and $ZrOCl_2·8H_2O$ (126 mg) were dissolved in 6 and 18 mL of DMF, respectively. After mixing the solutions above, 2 mL of CH_3COOH was added and allowed to react for 12 h at 120 °C to yield UiO-66 nanoparticles. The obtained UiO-66 nanoparticles were washed with DMF and CH_3CH_2OH for three times and then redispersed in 2 mL DMF before use.

Detection of Exosome. The hairpin oligonucleotides HP, HP1, and HP2 were folded into hairpin structure through heating at 95 °C for 5 min and then slowly cooled to room temperature before use. For target assay, 2.5 μM HP, 5 μM HP1, 5 μM HP2, 5 μM hemin, and 50 mM KCl were mixed with different concentrations of exosome and then added onto the Zr-MOFs-modified paper. After incubating at 37 °C for 80 min, 5 μM TMB and 0.6 mM H_2O_2 were added and incubated at room temperature for 6 min. Subsequently, the Zr-MOFs-modified paper was folded onto the surface of SPE for electrochemical detection. For selectivity evaluation, four

https://doi.org/10.1021/acs.analchem.1c02286
Anal. Chem. 2021, 93, 11792−11799

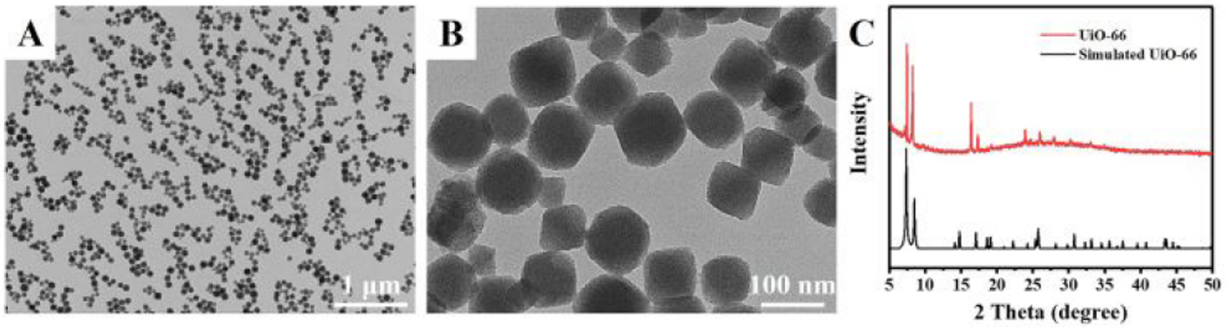

Figure 1. Low- and high-magnification TEM images (A, B) and XRD patterns (C) of the prepared and simulated UiO-66.

interfering substances, including 100 μg/mL of BSA, 100 μg/mL of lysozyme, 10 mM of glucose, and 10 mM of cysteine, were employed to replace exosome for electrochemical assay. Additionally, the mixtures of exosome (3.4×10^8 particles/mL) with each interfering biomolecule were also investigated by recoding their electrochemical responses under the same experimental conditions.

Cell Culture and Exosome Isolation. MCF-7 cells were cultured in PRMI 1640 medium. To produce exosomes, cells were transferred to a culture medium containing 10% exosome depleted FBS for 48 h. Then, cell and cell debris were first removed by centrifugation at 300 g for 10 min. Subsequently, the exosomes were isolated and purified by using the ExospinTM kit (Promega) according to the manufacturer's instruction. Finally, the collected exosomes were carefully resuspended in sterile PBS and stored at −80 °C for later experiments. The concentration of the exosomes was measured by using nanoparticle tracking analysis (NTA).

Other experimental details are described in the Supporting Information.

RESULTS AND DISCUSSION

Preparation and Characterization of MOFs and Paper-Based Biosensor. UiO-66 is a typical biocompatible Zr-MOF with zirconium ion as the metal nodes and terephthalate as the organic linkers. Owing to the rich zirconium ions on its surface and its high stability, UiO-66 was prepared and chosen to modify paper for capturing exosomes. The morphology and structure of the obtained MOFs were characterized by transmission electron microscopy (TEM) and X-ray diffraction (XRD), respectively. As displayed in Figure 1A,B and Figure S1, the size of UiO-66 nanoparticles was approximately 100 nm with uniform shape. The characteristic diffraction peaks of UiO-66 were highly consistent with the simulated pattern, indicating the successful synthesis of the Zr-MOFs nanoparticles (Figure 1C). The as-prepared MOFs were dropped on the surface of the paper. The morphology of the paper before and after modification of MOFs was characterized by using scanning electron microscopy (SEM). Compared with the untreated paper (Figure 2A,B), the SEM images showed that the MOFs nanoparticles were evenly dispersed on the surface of paper (Figure 2C−F, Figure S2). The Zr-MOFs modified paper was then pasted onto a soft plastic, which was used to link a disposable screen-printed electrode (SPE) for assembling a foldable electrochemical biosensor. In this sensor, Zr-MOFs modified paper was severed as the target recognition and signal amplification region, while SPE was employed as an electrochemical signal

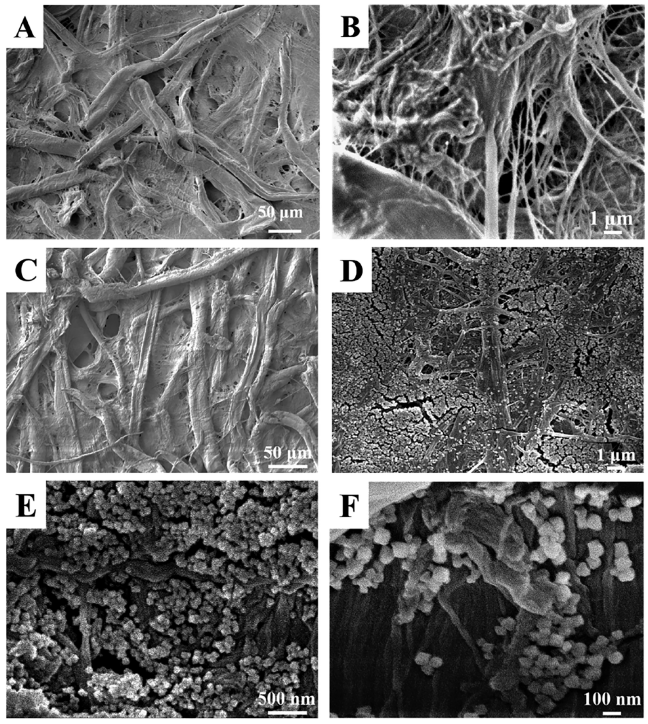

Figure 2. Low- and high-magnification SEM images of the paper before (A, B) and after the modification of Zr-MOFs (C−F).

readout element. The prepared biosensor was then used to detect tumor exosome.

Principle of the Biosensor for Exosome Assay. Figure 3 graphically illustrates the mechanism of the paper-based electrochemical biosensor for cancerous exosome assay. When exosomes and a reaction solution were added onto the MOFs-modified paper, exosomes would be adsorbed on the surface of Zr-MOFs through the formation of Zr−O−P bonds. At the same time, the reaction solution would recognize CD63 that is overexpressed on the membrane of MCF-7 derived exosomes to improve the determination selectivity. The reaction solution mainly contains three ingeniously designed hairpin probes, namely HP, HP1, and HP2. HP contains a CD63 aptamer sequence, which could bind to CD63 and trigger a conformational change of HP, exposing an occluded stem region. The newly released sticky region is partially complementary to the sequences embedded in the stem and loop of HP1. Thus, the unfolded HP would hybridize with part of HP1 and open it. Subsequently, the newly exposed single-stranded region in HP1 further hybridizes with the sticky end of HP2 to unfold it and expose a new sticky end on HP2, which, in turn, hybridizes

https://doi.org/10.1021/acs.analchem.1c02286
Anal. Chem. 2021, 93, 11792−11799

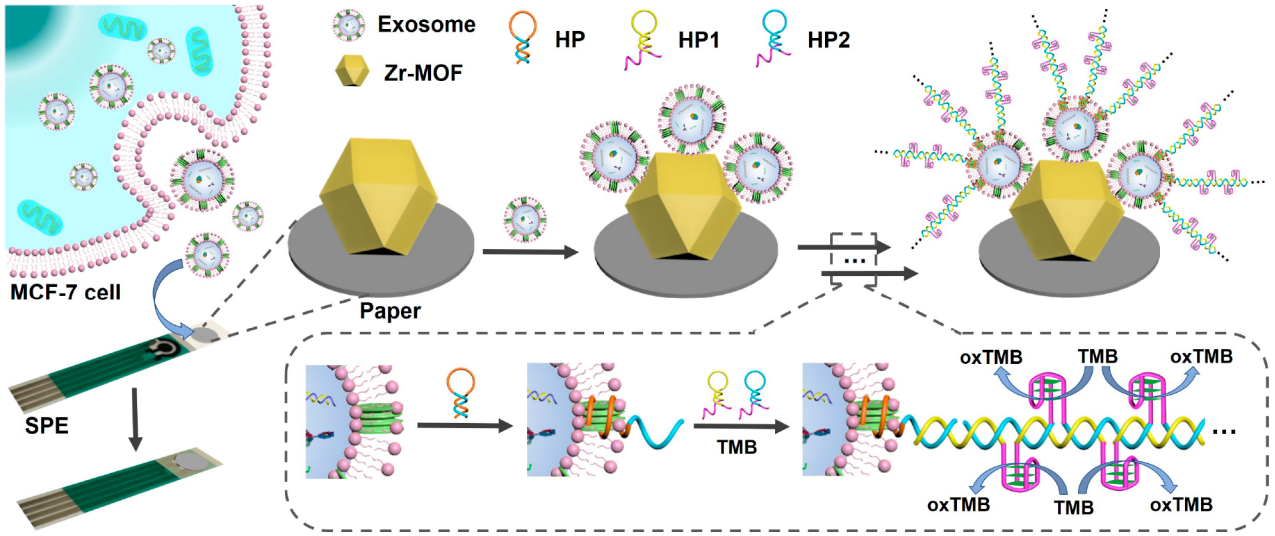

Figure 3. Principle of the paper-based biosensor for exosome assay.

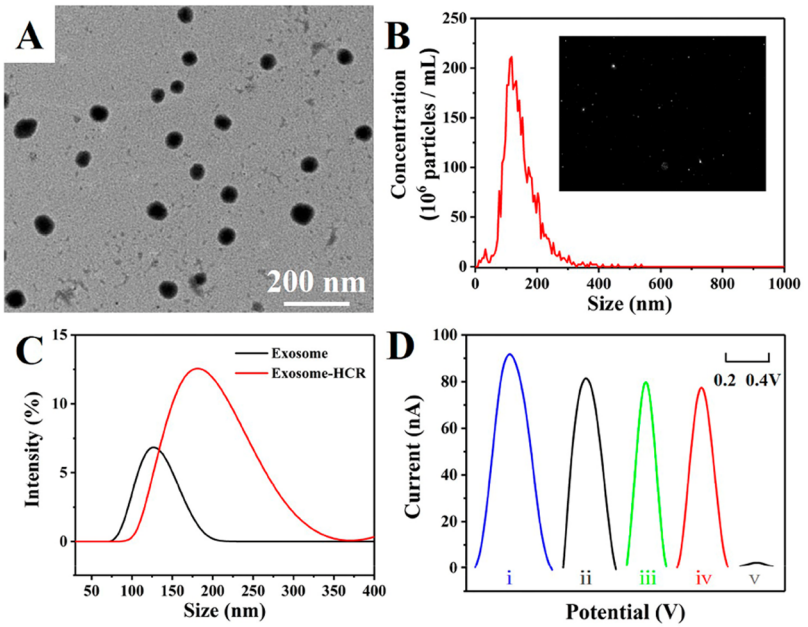

Figure 4. Characterization of MCF-7 cell-derived exosomes by (A) TEM and (B) NTA. Inset: a photograph taken in NTA assay. (C) Size distribution of the exosomes before and after HCR reaction measured by DLS. (D) DPV current of the biosensor response to the mixtures of (i) TMB and H_2O_2; (ii) TMB, H_2O_2, and hemin; (iii) TMB, H_2O_2, HP, HP1, and HP2; (iv) TMB, H_2O_2, hemin, HP, HP1, and HP2; (v) TMB, H_2O_2, hemin, HP, HP1, HP2, and exosome; the addition concentration of exosome is 3.4×10^8 particles/mL.

with another intact HP1. In this way, a cascade of hybridization between HP1 and HP2 occurs and produces long duplex DNA nanowires. In these nanowires, one chain is composed of multiple HP1s connected in a head-to-tail fashion, while another chain consists of multiple HP2s in the same fashion. Because the two ends of both HP1 and HP2 were designed to have split G-quadruplex (3:1) sequences, respectively, the two split G-quadruplex sequences at the head and tail of two adjacent HP1 (or HP2) would close to each other and form G-quadruplex structure. As a result, numerous G-quadruplexes were formed on both sides of the dsDNA nanowires. With the assistance of hemin, these G-quadruplexes display high catalytic activity toward TMB depletion. As previously reported, free TMB can diffuse to the surface of the electrode and produce an electrochemical response,[54] the oxidation of TMB on the Zr-MOFs modified paper leads to a decreased electrochemical signal on the SPE. In the absence of exosome, the HP, HP1, and HP2 are self-blocked, and the HCR procedure cannot occur. Thus, the TMB molecules can diffuse to the surface of electrode, generating a high electrochemical signal.

Feasibility Study. As a proof-of-concept, exosomes secreted from MCF-7 cells were employed as the model target. The isolated exosomes were validated by using TEM. As shown in Figure 4A, the exosomes are spherical vesicles with an average diameter of about 60 nm. Moreover, NTA was employed to measure the concentration and the size distribution of the collected exosomes. The concentration of exosome was found to be approximately 1.9×10^{10} particles/mL. The average hydrodynamic diameter was approximately

https://doi.org/10.1021/acs.analchem.1c02286
Anal. Chem. 2021, 93, 11792−11799

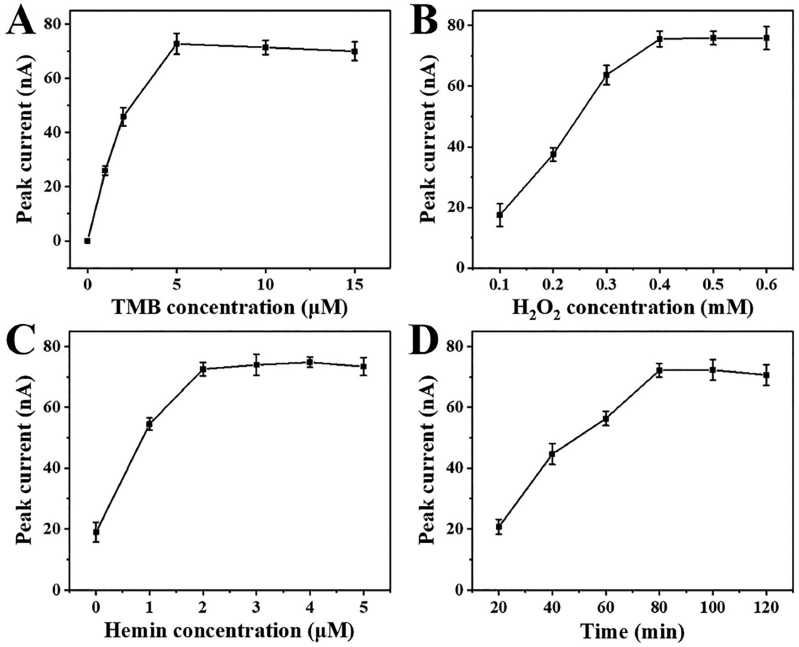

Figure 5. Optimization of the experimental conditions. DPV peak current intensities obtained under different conditions: (A) TMB concentrations: 0, 1, 2, 5, 10, and 15 μM; (B) H_2O_2 concentrations: 0.1, 0.2, 0.3, 0.4, 0.5, and 0.6 μM; (C) Hemin concentrations: 0, 1, 2, 3, 4, and 5 μM; (D) HCR reaction time: 20, 40, 60, 80, 100, and 120 min.

113 nm (Figure 4B), which was much higher than that displayed in the TEM image due to the optical scattering of solution.

To verify the exosome-initiated HCR process, dynamic light scattering (DLS) was utilized to monitor the size distribution of the exosome before and after incubating with HP, HP1, and HP2, respectively. As shown in Figure 4C, the average diameter of the exosome became larger after the HCR process, indicating the formation of long dsDNA nanowires on the surfaces of exosome. Furthermore, a broader size distribution range was observed, which was possibly attributed to the different lengths of the formed dsDNA nanowires. These results indicated the generation of dsDNA on exosomal surfaces via the HCR process. In addition to DLS, non-denaturing polyacrylamide gel electrophoresis (PAGE) was applied for validating the exosome-triggered HCR process (Figure S3), because the DNA sequences of HP, HP1, and HP2 were rationally and carefully designed to kinetically hinder any interaction between them without the exosome addition. As expected, a single and narrow electrophoresis band was observed for each hairpin DNA strand, including HP (lane i), HP1 (lane ii), and HP2 (lane iii). Although there are some complementary regions between them, no new band appeared after incubating all the above DNA strands (HP, HP1, and HP2) (lane iv), indicating the negligible interaction between each rationally designed hairpin structure in the absence of exosome. On the contrary, new bands with slower mobility emerged in the presence of exosome (lane v), implying the formation of DNA assemblies with higher molecular weight. Moreover, the new bands were broad, because the DNA nanowires produced by HCR process may have different length. These results demonstrated that the HCR process was successfully initiated in the presence of exosome.

The electrochemical property of the disposable SPE was investigated by cyclic voltammetry (CV). As shown in Figure S4A, a well-defined pair of redox peaks, which were corresponding to $Fe(CN)_6^{3-/4-}$, was observed on the bare SPE. The CV curves were almost unchanged after integrating SPE with paper and MOFs-modified paper to form a sensing element, indicating the negligible effect of paper and MOFs on the electrochemical behaviors of SPE. Additionally, the redox peaks increased regularly as the scan rate increased from 0.01 to 0.3 V/s (Figure S4B), and both the oxidation peak current (i_{pa}) and reduction peak current (i_{pc}) exhibited good linear relationships with the square root of the scan rates ($v^{1/2}$), implying a typical diffusion-controlled processes (Figure S4C).

The feasibility of the proposed paper-based biosensor for exosome assay was verified by measuring the electrochemical response of the biosensor under different experimental conditions. As shown in Figure 4D, the mixed solution of TMB and H_2O_2 generated a high differential pulse voltammetry (DPV) current on the SPE (curve i). Furthermore, the DPV response of TMB almost unchanged when hemin (curve ii) or the mixture of HP, HP1, and HP2 (curve iii) were added, indicating that hemin, HP, HP1, and HP2 have no obvious influence on the electrochemical response. Additionally, similar results were observed in the presence of hemin, HP, HP1, and HP2 (curve iv), demonstrating that no G-quadruplex DNAzyme was formed, and the HCR process was not triggered in the absence of exosome. In contrast, a weak current was obtained in the presence of exosome and other reagents (curve v). These results indicated that the HCR process was initiated by the target exosome, which led to the oxidation of TMB on the paper surface. Thus, no obvious electrochemical signal of TMB was observed on the SPE.

Optimization of Experimental Conditions. Before using the paper-based biosensor for exosome assay, some experimental parameters, including the concentration of TMB, hemin, H_2O_2, and the reaction time, were optimized to obtain a good analytical performance. As the signal molecules, the

https://doi.org/10.1021/acs.analchem.1c02286
Anal. Chem. 2021, 93, 11792−11799

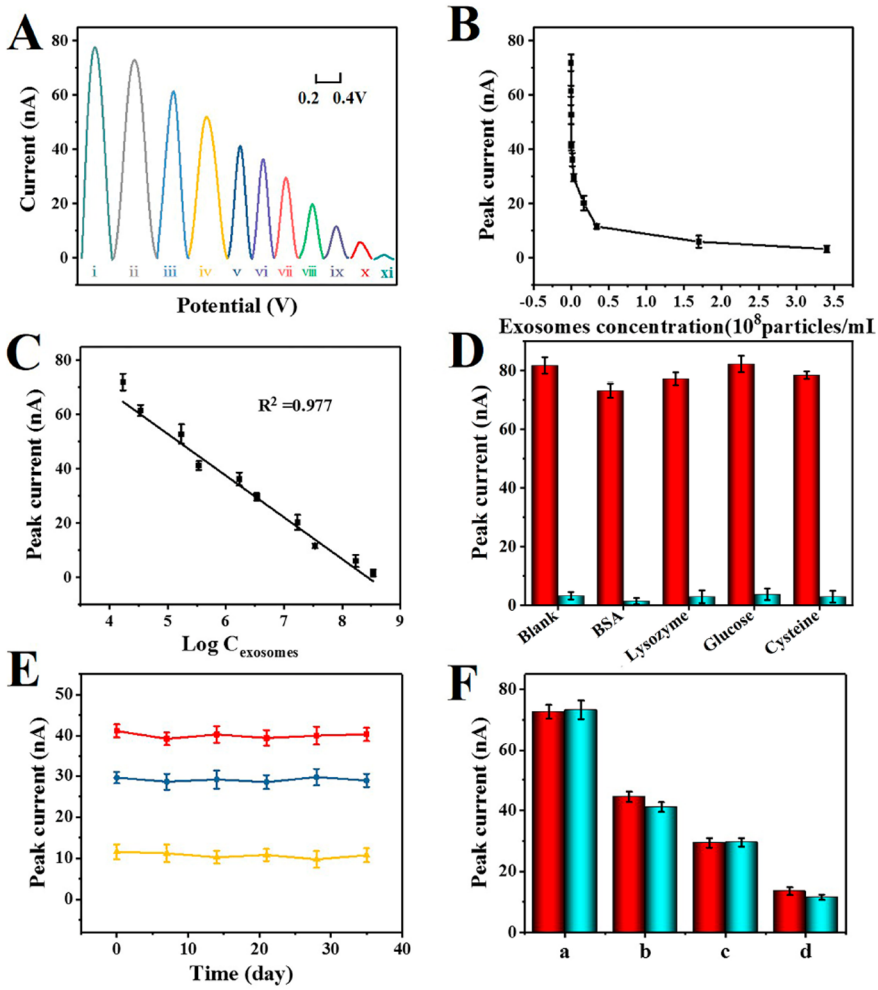

Figure 6. (A) DPV current obtained from different concentrations of exosomes: (i–xi) 0, 1.7×10^4, 3.4×10^4, 1.7×10^5, 3.4×10^5, 1.7×10^6, 3.4×10^6, 1.7×10^7, 3.4×10^7, 1.7×10^8, and 3.4×10^8 particles/mL, respectively. (B) Relationship between DPV peak current intensity and the exosome concentration. (C) Linear relationship between the peak current intensity and the logarithm of exosome concentration. (D) DPV peak current intensity of the biosensor in the absence (blank) and presence of different interfering substances (red column): BSA, lysozyme, glucose, cysteine, and their mixtures with exosomes (cyan column), respectively. (E) DPV peak current intensity of the paper-based biosensor response to (i) 3.4×10^5, (ii) 3.4×10^6, and (iii) 3.4×10^7 particles/mL of exosome after storage of the biosensor at room temperature for different days: 0, 7, 14, 21, 28, and 35 days. (F) DPV peak current intensities obtained from FBS samples (red column) and buffer (cyan column) with the added concentration of exosome are (a–d) 0, 3.4×10^5, 3.4×10^6, and 3.4×10^7 particles/mL, respectively.

concentration of TMB has a strong influence on the electrochemical response. As shown in Figure 5A, the peak current of the biosensor was dramatically increased with the concentration of TMB increased from 0 to 5 μM, while further increasing the TMB concentration led to a slight decrease of the DPV signal. Thus, 5 μM was chosen as the optimum TMB concentration. Figure 5B shows the effect of H_2O_2 concentration on the electrochemical response. Evidently, the DPV peak currents increased dramatically as the concentration of H_2O_2 increased from 0.1 to 0.4 mM. Then, the DPV peak current reached a plateau when the concentration was further elevated to 0.6 mM, indicating that the optimum concentration for H_2O_2 is 0.4 mM. Since hemin is an essential component of DNAzyme that affects its catalytical activity, the concentration of hemin was optimized. As can be seen from Figure 5C, a higher DPV peak current was observed when an elevated hemin concentration was adopted in the range from 0 to 2 μM. Then, the peak current was almost unchanged as the concentration of hemin increased to 5 μM, indicating that 2 μM is the optimum hemin concentration. Moreover, the effect of reaction time on the DPV response was also investigated, and the results were displayed in Figure 5D. Obviously, the peak currents increased gradually as the reaction time increased from 20 to 80 min. However, the DPV peak current was slightly decreased with the extension of the reaction time up to 120 min. Thus, 80 min was selected as the optimal reaction time.

Analytical Performance of the Paper-Based Biosensor. Under the optimal experimental conditions, the analytical performance of the paper-based biosensor was investigated by recording the DPV signals in the presence of MCF-7 cell-derived exosomes. As shown in Figure 6A, the DPV current of TMB gradually decreased as the amount of exosome increased, implying that the formation of dsDNA nanowires and G-quadruplex DNAzymes was highly dependent on the concentration of exosome. The detailed relationship between the DPV peak current intensity and the amount of exosome was depicted in Figure 6B. Obviously, exosomes could be directly detected in the range from 1.7×10^4 to 3.4×10^8 particles/mL. Furthermore, a good linear electrochemical

https://doi.org/10.1021/acs.analchem.1c02286
Anal. Chem. 2021, 93, 11792–11799

response was obtained between the peak current intensity and the logarithm of exosome concentration (Figure 6C). The correlation equation is i_p = 129.7−15.4 log $C_{exosome}$ (R^2 = 0.977), where i_p is the DPV peak current intensity (nA) and $C_{exosome}$ is the exosome concentration (particles/mL). The limit of detection (LOD) was calculated to be 5 × 10^3 particles/mL, which was comparable to or superior than that of most previously reported methods (Table S1). These results confirmed that the paper-based POC biosensor was efficient for highly sensitive determination of exosomes.

Moreover, the specificity of the paper-based biosensor was investigated by replacing exosomes with some possible interfering substances in serum samples, including BSA, lysozyme, glucose, and cysteine. As shown in Figure 6D, these interfering substances had similar DPV signals to those of the blank sample. On the contrary, remarkable decreased DPV signals were obtained when these biomolecules were mixed with exosomes, indicating the excellent selectivity of the proposed sensing platform. Besides, the stability of the proposed POC biosensor was evaluated by measuring the DPV signals toward 3.4 × 10^5, 3.4 × 10^6, and 3.4 × 10^7 particles/mL exosome after storing different days (Figure 6E). For all the three exosome concentrations, the electrochemical signals were almost unchanged after storing for 5 weeks at room temperature, implying the high stability of the proposed paper-based biosensor.

Determination of Exosome in Biological Samples. The practicability of the paper-based biosensor for analyzing cancer-derived exosomes in biological samples was evaluated by detecting tumor exosomes contained in exosome-free fetal bovine serum (FBS). After spiking various concentrations of MCF-7 cell-derived exosomes into 10% diluted FBS, the electrochemical response of the paper-based biosensor toward the spiked samples was measured and compared with the unspiked samples. As shown in Figure 6F, the examined DPV current intensities of the exosome-spiked FBS were close to that of the buffer solution with the same exosome concentration, respectively. The recoveries for exosome were 95%, 97%, and 102%, respectively (Table S2). Thus, the proposed paper-based biosensor was feasible for measuring exosome in biological environment.

CONCLUSIONS

In summary, a label-free and enzyme-free paper-based POC biosensor was developed for portable, sensitive, and quantitative determination of cancer-derived exosomes by using Zr-MOFs and aptamer as the recognition system along with HCR and DNAzyme-mediated catalysis for signal amplification. Through the recognition of exosomes by Zr-MOFs and aptamer, HCR was triggered for the formation of G-quadruplex DNAzymes, which converted the exosome assay to a DNAzyme-catalyzed signal amplification. Taking advantage of the high signal amplification ability of HCR and the high catalytical effect of DNAzyme, this paper-based electrochemical biosensor enabled highly sensitive determination of exosome with a LOD down to 5 × 10^3 particles/mL. Furthermore, the paper-based biosensor that constructed by Zr-MOF modified paper and a commercial SPE possessed the features of inexpensive, simple operation, high sensitivity, making it affordable and user-friendly for POC diagnosis in resource-limited settings.

ASSOCIATED CONTENT

Supporting Information

The Supporting Information is available free of charge at https://pubs.acs.org/doi/10.1021/acs.analchem.1c02286.

Supplementary experimental section: chemicals and materials; instruments; preparation of test paper; gel electrophoresis analysis; detection of exosome in FBS samples. Supporting tables: comparison of the present method with reported methods; recovery data for exosome spiked FBS samples. Supporting figures: TEM images of the Zr-MOFs; SEM images of the Zr-MOFs modified paper; PAGE analysis of the sensing system; electrochemical properties of SPE (PDF)

AUTHOR INFORMATION

Corresponding Author

Feng Li − *College of Chemistry and Pharmaceutical Sciences, Qingdao Agricultural University, Qingdao 266109, P. R. China*; orcid.org/0000-0002-3894-6139; Email: lifeng@qau.edu.cn

Authors

Xiaojuan Liu − *College of Chemistry and Pharmaceutical Sciences, Qingdao Agricultural University, Qingdao 266109, P. R. China*

Xin Gao − *College of Chemistry and Pharmaceutical Sciences, Qingdao Agricultural University, Qingdao 266109, P. R. China*

Limin Yang − *College of Chemistry and Pharmaceutical Sciences, Qingdao Agricultural University, Qingdao 266109, P. R. China*

Yuecan Zhao − *College of Chemistry and Pharmaceutical Sciences, Qingdao Agricultural University, Qingdao 266109, P. R. China*

Complete contact information is available at: https://pubs.acs.org/10.1021/acs.analchem.1c02286

Notes

The authors declare no competing financial interest.

ACKNOWLEDGMENTS

This work was financially supported by the National Natural Science Foundation of China (Nos. 21775083, 21804077, 22076090), the Special Foundation for Distinguished Taishan Scholar of Shandong Province (No. ts201511052), the Postgraduate Innovation Program of Qingdao Agricultural University (QNYCX20017).

REFERENCES

(1) Kalluri, R.; LeBleu, V. S. *Science* **2020**, *367*, 6478.
(2) Shao, B.; Xiao, Z. *Anal. Chim. Acta* **2020**, *1114*, 74−84.
(3) Zhao, L.; Sun, R.; He, P.; Zhang, X. *Anal. Chem.* **2019**, *91*, 14773−14779.
(4) Zhang, P.; He, M.; Zeng, Y. *Lab Chip* **2016**, *16*, 3033−3042.
(5) Lyu, Y.; Cui, D.; Huang, J.; Fan, W.; Miao, Y.; Pu, K. *Angew. Chem., Int. Ed.* **2019**, *58*, 4983−4987.
(6) Johnsen, K. B.; Gudbergsson, J. M.; Skov, M. N.; Pilgaard, L.; Moos, T.; Duroux, M. *Biochim. Biophys. Acta, Rev. Cancer* **2014**, *1846*, 75−87.
(7) Tkach, M.; Thery, C. *Cell* **2016**, *164*, 1226−1232.
(8) Whiteside, T. L. *Adv. Clin. Chem.* **2016**, *74*, 103−141.
(9) Xu, R.; Rai, A.; Chen, M.; Suwakulsiri, W.; Greening, D. W.; Simpson, R. J. *Nat. Rev. Clin. Oncol.* **2018**, *15*, 617−638.

(10) Cheng, N.; Du, D.; Wang, X.; Liu, D.; Xu, W.; Luo, Y.; Lin, Y. *Trends Biotechnol.* **2019**, *37*, 1236−1254.
(11) Jin, D.; Yang, F.; Zhang, Y. L.; Liu, L.; Zhou, Y. J.; Wang, F. B.; Zhang, G. J. *Anal. Chem.* **2018**, *90*, 14402−14411.
(12) Lee, J.; Kim, H.; Heo, Y.; Yoo, Y. K.; Han, S. I.; Kim, C.; Hur, D.; Kim, H.; Kang, J. Y.; Lee, J. H. *Analyst* **2020**, *145*, 157−164.
(13) Liu, W.; Li, J.; Wu, Y.; Xing, S.; Lai, Y.; Zhang, G. *Biosens. Bioelectron.* **2018**, *102*, 204−210.
(14) Tian, Q.; He, C.; Liu, G.; Zhao, Y.; Hui, L.; Mu, Y.; Tang, R.; Luo, Y.; Zheng, S.; Wang, B. *Anal. Chem.* **2018**, *90*, 6556−6562.
(15) Liu, C.; Zhao, J.; Tian, F.; Chang, J.; Zhang, W.; Sun, J. *J. Am. Chem. Soc.* **2019**, *141*, 3817−3821.
(16) Jiang, Y.; Shi, M.; Liu, Y.; Wan, S.; Cui, C.; Zhang, L.; Tan, W. *Angew. Chem., Int. Ed.* **2017**, *56*, 11916−11920.
(17) Wan, S.; Zhang, L.; Wang, S.; Liu, Y.; Wu, C.; Cui, C.; Sun, H.; Shi, M.; Jiang, Y.; Li, L.; Qiu, L.; Tan, W. *J. Am. Chem. Soc.* **2017**, *139*, 5289−5292.
(18) Guo, Y.; Cao, Q.; Feng, Q. *Anal. Chim. Acta* **2020**, *1135*, 55−63.
(19) Miao, P.; Tang, Y. *Chem. Commun.* **2020**, *56*, 4982−4985.
(20) Wang, H.; Wan, K.; Zhou, Y.; He, X.; He, D.; Cheng, H.; Huang, J.; Jia, R.; Wang, K. *Chem. Commun.* **2020**, *56*, 12949−12952.
(21) Yu, Y.; Zhang, W. S.; Guo, Y.; Peng, H.; Zhu, M.; Miao, D.; Su, G. *Biosens. Bioelectron.* **2020**, *167*, 112482.
(22) He, F.; Wang, J.; Yin, B. C.; Ye, B. C. *Anal. Chem.* **2018**, *90*, 8072−8079.
(23) Xu, L.; Chopdat, R.; Li, D.; Al-Jamal, K. T. *Biosens. Bioelectron.* **2020**, *169*, 112576.
(24) Yang, Y.; Li, C.; Shi, H.; Chen, T.; Wang, Z.; Li, G. *Talanta* **2019**, *192*, 325−330.
(25) Pan, Y.; Wang, L.; Deng, Y.; Wang, M.; Peng, Y.; Yang, J.; Li, G. *Chem. Commun.* **2020**, *56*, 13768−13771.
(26) Lin, B.; Tian, T.; Lu, Y.; Liu, D.; Huang, M.; Zhu, L.; Zhu, Z.; Song, Y.; Yang, C. *Angew. Chem., Int. Ed.* **2021**, *60*, 7582−7586.
(27) Im, H.; Shao, H.; Park, Y. I.; Peterson, V. M.; Castro, C. M.; Weissleder, R.; Lee, H. *Nat. Biotechnol.* **2014**, *32*, 490−495.
(28) Zhu, L.; Wang, K.; Cui, J.; Liu, H.; Bu, X.; Ma, H.; Wang, W.; Gong, H.; Lausted, C.; Hood, L.; Yang, G.; Hu, Z. *Anal. Chem.* **2014**, *86*, 8857−8864.
(29) Picciolini, S.; Gualerzi, A.; Vanna, R.; Sguassero, A.; Gramatica, F.; Bedoni, M.; Masserini, M.; Morasso, C. *Anal. Chem.* **2018**, *90*, 8873−8880.
(30) Stremersch, S.; Marro, M.; Pinchasik, B. E.; Baatsen, P.; Hendrix, A.; De Smedt, S. C.; Loza-Alvarez, P.; Skirtach, A. G.; Raemdonck, K.; Braeckmans, K. *Small* **2016**, *12*, 3292−3301.
(31) Almughlliq, F. B.; Koh, Y. Q.; Peiris, H. N.; Vaswani, K.; McDougall, S.; Graham, E. M.; Burke, C. R.; Arachchige, B. J.; Reed, S.; Mitchell, M. D. *Theriogenology* **2018**, *114*, 173−179.
(32) Oliveira-Rodríguez, M.; Serrano-Pertierra, E.; García, A. C.; López-Martín, S.; Yañez-Mo, M.; Cernuda-Morollón, E.; Blanco-López, M. D. C. *Biosens. Bioelectron.* **2017**, *87*, 38−45.
(33) Zhang, Y. Z.; Jiao, J. Y.; Wei, Y. Y.; Wang, D. N.; Yang, C. G.; Xu, Z. R. *Anal. Chem.* **2020**, *92*, 15244−15252.
(34) Boriachek, K.; Masud, M. K.; Palma, C.; Phan, H. P.; Yamauchi, Y.; Hossain, M. S.; Nguyen, A. N. T.; Salomon, C.; Shiddiky, M. J. A. *Anal. Chem.* **2019**, *91*, 3827−3834.
(35) Bruch, R.; Johnston, M.; Kling, A.; Mattmüller, T.; Baaske, J.; Partel, S.; Madlener, S.; Weber, W.; Urban, G. A.; Dincer, C. *Biosens. Bioelectron.* **2021**, *177*, 112887.
(36) Bagheri Hashkavayi, A.; Cha, B. S.; Lee, E. S.; Kim, S.; Park, K. S. *Anal. Chem.* **2020**, *92*, 12733−12740.
(37) Liu, X.; Li, X.; Gao, X.; Ge, L.; Sun, X.; Li, F. *ACS Appl. Mater. Interfaces* **2019**, *11*, 15381−15388.
(38) Gao, X.; Li, X.; Sun, X.; Zhang, J.; Zhao, Y.; Liu, X.; Li, F. *Anal. Chem.* **2020**, *92*, 4592−4599.
(39) Wang, S.; Zhang, L.; Wan, S.; Cansiz, S.; Cui, C.; Liu, Y.; Cai, R.; Hong, C.; Teng, I. T.; Shi, M.; Wu, Y.; Dong, Y.; Tan, W. *ACS Nano* **2017**, *11*, 3943−3949.
(40) Kashefi-Kheyrabadi, L.; Kim, J.; Chakravarty, S.; Park, S.; Gwak, H.; Kim, S. I.; Mohammadniaei, M.; Lee, M. H.; Hyun, K. A.; Jung, H. I. *Biosens. Bioelectron.* **2020**, *169*, 112622.
(41) Yin, X.; Hou, T.; Huang, B.; Yang, L.; Li, F. *Chem. Commun.* **2019**, *55*, 13705−13708.
(42) Yang, L.; Yin, X.; An, B.; Li, F. *Anal. Chem.* **2021**, *93*, 1709−1716.
(43) Yang, X.; Tang, Q.; Jiang, Y.; Zhang, M.; Wang, M.; Mao, L. *J. Am. Chem. Soc.* **2019**, *141*, 3782−3786.
(44) Chang, J.; Wang, X.; Wang, J.; Li, H.; Li, F. *Anal. Chem.* **2019**, *91*, 3604−3610.
(45) Liu, X.; Zhao, Y.; Li, F. *Biosens. Bioelectron.* **2021**, *173*, 112832.
(46) Li, X.; Gao, X.; Gai, P.; Liu, X.; Li, F. *Sens. Actuators, B* **2020**, *323*, 128701.
(47) Sun, Z.; Wu, S.; Ma, J.; Shi, H.; Wang, L.; Sheng, A.; Yin, T.; Sun, L.; Li, G. *ACS Appl. Mater. Interfaces* **2019**, *11*, 36316−36323.
(48) Wang, Z.; Fu, Y.; Kang, Z.; Liu, X.; Chen, N.; Wang, Q.; Tu, Y.; Wang, L.; Song, S.; Ling, D.; Song, H.; Kong, X.; Fan, C. *J. Am. Chem. Soc.* **2017**, *139*, 15784−15791.
(49) Wang, S.; McGuirk, C. M.; Ross, M. B.; Wang, S.; Chen, P.; Xing, H.; Liu, Y.; Mirkin, C. A. *J. Am. Chem. Soc.* **2017**, *139*, 9827−9830.
(50) Liu, Y.; Hou, W.; Xia, L.; Cui, C.; Wan, S.; Jiang, Y.; Yang, Y.; Wu, Q.; Qiu, L.; Tan, W. *Chem. Sci.* **2018**, *9*, 7505−7509.
(51) Sun, Z.; Wang, L.; Wu, S.; Pan, Y.; Dong, Y.; Zhu, S.; Yang, J.; Yin, Y.; Li, G. *Anal. Chem.* **2020**, *92*, 3819−3826.
(52) Gu, C.; Bai, L.; Pu, L.; Gai, P.; Li, F. *Biosens. Bioelectron.* **2021**, *176*, 112907.
(53) Wang, L.; Yang, Y.; Liu, Y.; Ning, L.; Xiang, Y.; Li, G. *Chem. Commun.* **2019**, *55*, 2708−2711.
(54) Sun, Q.; Yan, F.; Su, B. *Biosens. Bioelectron.* **2018**, *105*, 129−136.

https://doi.org/10.1021/acs.analchem.1c02286
Anal. Chem. 2021, 93, 11792−11799